PROCEEDINGS of the
23rd International Congress on Acoustics
9 to 13 September 2019 in Aachen, Germany

Non-reciprocity in discrete and continuous lattice systems via mechanical modulation

Benjamin M. Goldsberry[(1)], Samuel P. Wallen[(1)], Michael R. Haberman[(1)]

[(1)]Walker Department of Mechanical Engineering and Applied Research Laboratories, The University of Texas at Austin, Austin, TX, USA

Abstract

Materials with time- and space-dependent effective properties are of significant interest as a means to introduce non-reciprocal wave propagation in engineered material systems. Materials displaying this unique behavior have significant potential as direction- dependent devices for mechanical wave sensing and transmitting capabilities. They also open up the possibility for the construction of novel materials or structures that isolate unwanted vibration. Recent analytical models of spring-mass chains have shown that external application of a nonlinear mechanical deformation, when applied on time scales that are slow compared to the characteristic times of propagating linear elastic waves, may induce non-reciprocity via changes in the apparent elastic modulus for perturbations around that deformation [Wallen et al., Phys.Rev. E., 99, 013001, (2019)]. This work investigates direct numerical simulation of discrete lattices and a finite element approach for continuous elastic systems to simulate elastic wave propagation in mechanically-modulated metamaterials. Analysis of the degree of non-reciprocity when varying sub-wavelength geometry or geometric modulations will be shown. Of specific interest is the use of FEM to investigate non- reciprocity in elastic lattices consisting of unit cells with varied geometric asymmetry and more general forms of mechanical modulation.

Keywords: Elastic waves, Metamaterials, Non-reciprocity

1 INTRODUCTION

Acoustic systems that break reciprocity have recently received great attention due to their potential to increase control over wave propagation and to create devices that make use of acoustic or elastic waves. Tools for the modeling, design, and analysis of media that generates non-reciprocal wave propagation have strong potential for far-reaching impacts on engineering applications, including more efficient acoustic communication and imaging devices, analogue signal processing, and vibration isolation. One means to break reciprocity is through spatiotemporal modulation of material properties [1]. Recent analytical models of spring-mass chains have shown that external application of a nonlinear mechanical deformation, when applied on time scales that are slow compared to the characteristic times of propagating linear elastic waves, may induce non-reciprocity via changes in the linearized local elastic modulus for perturbations around that deformation [2].

In a recent work, we investigated a continuous tunable mechanical metamaterial structure as a platform to achieve non-reciprocity [3]. A computational approach based on the finite element method was derived and implemented due to the complex unit cell geometry used to obtain large effective dynamic property modulations. In this work, we revisit the derivation of our computational approach by characterizing wave propagation in a medium with space-only and time-only modulation of the material modulus, and determining how these concepts generalize to the case of spatiotemporal modulation of the material modulus. Our analysis is implemented in a one-dimensional setting to compare with known exact solutions. Longitduinal wave propagation in a bar is used as an example case for each study.

2 WAVE PROPAGATION IN A MODULATED MEDIUM

The partial differential equation that describes wave propagation in a modulated medium is the one-dimensional wave equation of the form

$$\frac{\partial}{\partial x}\left(a(x,t)\frac{\partial u}{\partial x}\right) - b\frac{\partial^2 u}{\partial t^2} = 0, \quad -\infty < x < \infty, \quad t \geq 0, \tag{1}$$

with coefficient $a(x,t) > 0$ that is a non-constant function of time and space, and coefficient $b > 0$ that is assumed to be constant. Equation (1) can be used to represent various well-studied physical systems, such as longitudinal wave propagation in a bar. The dependent variable $u(x,t)$ is then the longitudinal particle displacement of the bar, $a(x,t) = E(x,t)$ is the Young's modulus, and $b = \rho_0$ is the mass per unit volume of the bar.

It is assumed that there is a reference modulation length, λ_m, in which $a(x,t)$ is periodic in space for all time,

$$a(x+\lambda_\mathrm{m},t) = a(x,t), \tag{2}$$

and a reference time T_m with angular frequency $\omega_\mathrm{m} = 2\pi/T_\mathrm{m}$ in which $a(x,t)$ is periodic in time for all locations in space, i.e.

$$a(x,t+T_\mathrm{m}) = a(x,t). \tag{3}$$

Therefore, Bloch-Floquet wave theory can be utilized to derive differential equations, which can be solved for the allowable traveling-wave modes and their respective dispersion behavior, or frequency-wavenumber spectrum [4]. Solution procedures for Eq. (1) with space-only, time-only, and space-time modulation of $a(x,t)$ are now derived that are computationally feasible and yield accurate calculations of the Bloch wave modes and dispersion relations.

2.1 Space-dependent modulus

Consider a modulus that is a function of space only, $a(x,t) \to a(x)$. This case physically represents a periodic heterogeneous medium, which is a common acoustic metamaterial structure and is frequently referred to as a phononic crystal [5, 6]. The traveling wave solution has the following form

$$u(x,t) = C\hat{u}(x)e^{\mathrm{i}(kx-\omega t)}, \tag{4}$$

where C is the amplitude constant, $\hat{u}(x)$ is the Bloch wave mode that is a periodic function on the unit cell domain of the phononic crystal, k is the Bloch wavenumber, and ω is the Bloch wave angular frequency. The finite element method has been used in previous works to successfully solve Bloch wave problems of this type, which leads to a generalized eigenvalue problem of the form [7]

$$\left(\mathbf{K}(k) - \omega^2\mathbf{M}\right)\hat{\boldsymbol{u}} = 0, \tag{5}$$

where $\mathbf{K}$ is the stiffness matrix which is a function of the Bloch wavenumber, $\mathbf{M}$ is the mass matrix, and $\hat{\boldsymbol{u}}$ is the Bloch wave mode that is discretized in space on a computational mesh. The dispersion relation $\omega(k)$ is solved by sweeping k in the first Brillouin zone and solving Eq. (5) for ω.

As an example case, consider longitudinal wave propagation in a bar composed of two periodically-alternating material layers with identical density $b = \rho_0$. The first layer has Young's modulus E_1 and thickness L_1, and the second layer has Young's modulus E_2 and thickness L_2. The periodic interval has length $L = L_1 + L_2 = \lambda_m$ and unit cell defined at $-L/2 \leq x \leq L/2$. Assume, without loss of generality of the method, that the two layers have the same thickness, $L_1 = L_2$. The modulus $a(x) = E(x)$ is therefore defined as the piecewise function

$$E(x) = \begin{cases} E_1, & \text{if } -\frac{L}{2} \leq x < 0, \\ E_2, & \text{if } 0 \leq x < \frac{L}{2}. \end{cases} \tag{6}$$

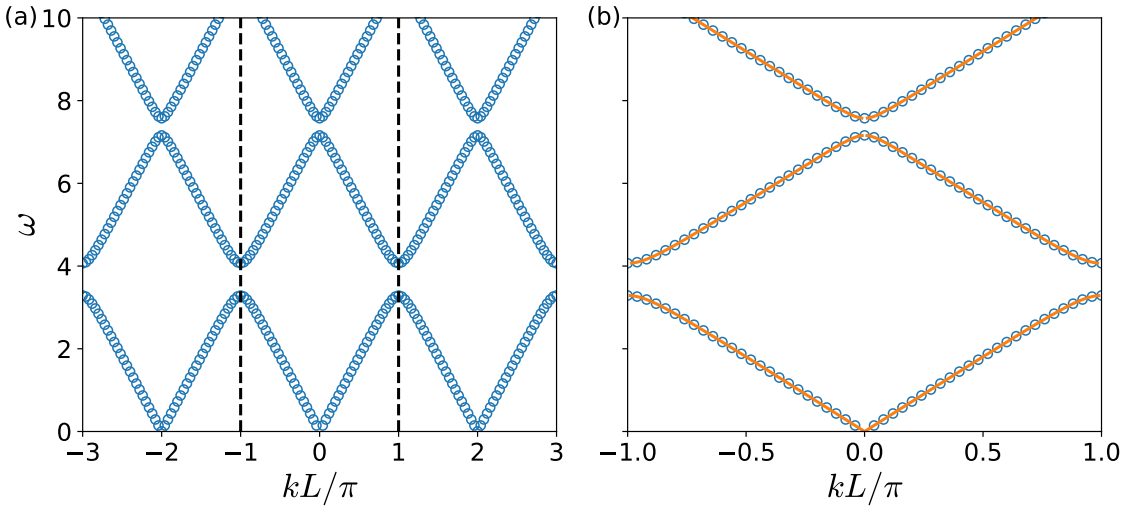

Figure 1. (a) Finite element computation of the dispersion relation for propagating longitudinal waves in a bar with periodic alternating layers. Since the dispersion relation is periodic, the complete dispersion relation can be obtained by restricting k to lie within the first Brillouin zone (black dashed lines). (b) Comparison of the finite element computation in the first Brillouin zone from (a) with the exact dispersion relation (orange lines), Eq. (7).

The exact dispersion relation in this case is the equation [4]

$$\cos(kL) = \cos\left(\frac{\omega}{c_1}L_1\right)\cos\left(\frac{\omega}{c_2}L_2\right) - \frac{1}{2}\left(\frac{z_1}{z_2}+\frac{z_2}{z_1}\right)\sin\left(\frac{\omega}{c_1}L_1\right)\sin\left(\frac{\omega}{c_2}L_2\right), \tag{7}$$

where $c_{1,2} = \sqrt{E_{1,2}/\rho_0}$ is the sound speed in each layer, and $z_{1,2} = \rho_0 c_{1,2}$ is the impedance of each layer. Figure 1(a) shows the resulting eigenfrequencies from the finite element calculation using the properties $E_1 = 1$, $E_2 = 2$, $\rho_0 = 1$, $L = 1$, and Fig. 1(b) compares the finite element results with the exact dispersion relation provided by Eq. (7). Excellent agreement is obtained between the exact dispersion relation and the finite element simulation. As a consequence of the Bloch-Floquet theory, the dispersion relation is periodic with wavenumber periodicity $\omega(k+k_L) = \omega(k)$, where $k_L = 2\pi/L$. The complete dispersion curve can therefore be obtained by limiting k to the first Brillouin zone, which is the range $k \in [-\pi/L, \pi/L]$ and is denoted by the vertical dashed lines in Fig. 1(a) [4]. In addition, the periodicity of the layers gives rise to Bragg scattering, in which the scattered waves caused by the impedance mismatch between the layers destructively interferes with the traveling wave in certain frequency bands [8, 9]. This interference creates bandgaps in the dispersion relation, which prohibits traveling waves with frequencies within the gap. The widths of the bandgaps are a function of the contrast of the material moduli $\Delta E = E_2 - E_1$.

2.2 Time-dependent modulus

Now consider the case where the modulus is a periodic function of time, $a(x,t) \to a(t)$. For this case, Eq. (1) reduces to

$$a(t)\frac{\partial^2 u}{\partial x^2} - b\frac{\partial^2 u}{\partial t^2} = 0. \tag{8}$$

The traveling wave solution to Eq. (8) has the following form

$$u(x,t) = C\Phi(t)e^{\mathrm{i}(kx-\omega t)}. \tag{9}$$

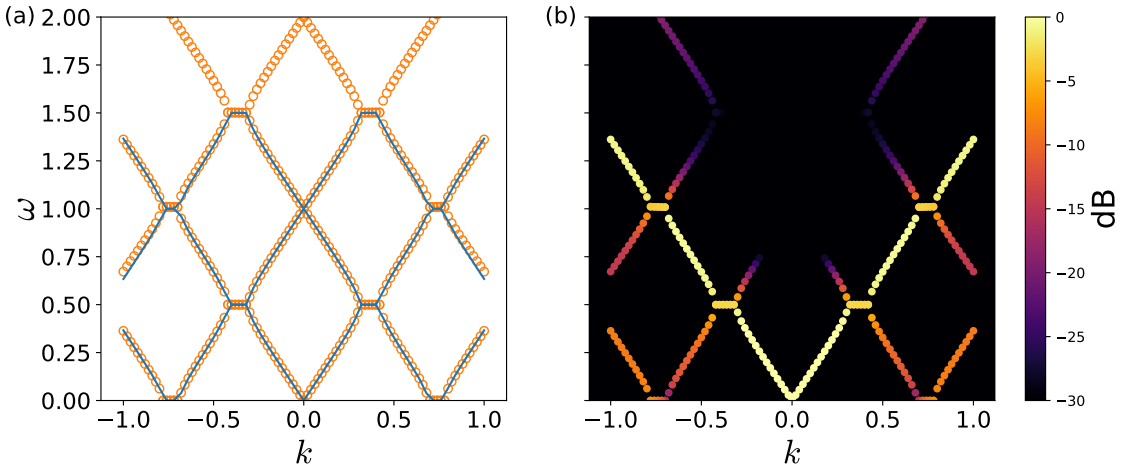

Figure 2. (a) Comparison of the frequency-wavenumber spectrum using Eq. (13) (open circles) with the exact dispersion solution, Eq. (17). (b) Dispersion relation from (a) weighted by the magnitude of the fundamental plane wave component in decibels, $20\log_{10}(||\hat{\Phi}_0||/||\hat{\mathbf{\Phi}}||)$.

Note that Eq. (9) has the same form as Eq. (4), except the Bloch function in Eq. (9) is now a periodic function of time. Since $a(t)$ is assumed to be periodic with frequency $\omega_\mathrm{m} = 2\pi/T_\mathrm{m}$, $a(t)$ can be written as a Fourier series in time,

$$a(t) = \sum_{n=-N}^{N} \hat{a}_n e^{-in\omega_\mathrm{m} t}, \tag{10}$$

where it is assumed that the function $a(t)$ can be well-represented with $2N+1$ Fourier terms. The coefficients $\hat{a}_n$ are determined by the Fourier integral

$$\hat{a}_n = \frac{\omega_\mathrm{m}}{2\pi} \int_{-\pi/\omega_\mathrm{m}}^{\pi/\omega_\mathrm{m}} a(t) e^{in\omega_\mathrm{m} t}. \tag{11}$$

Likewise, $\Phi(t)$ can also be expanded as a Fourier series in time,

$$\Phi(t) = \sum_{m=-N}^{N} \hat{\Phi}_m e^{-im\omega_\mathrm{m} t}. \tag{12}$$

Substitution of Eqns. (10) and (12) into Eq. (8) and utilizing orthogonality of the Fourier series yields a quadratic eigenvalue problem,

$$\omega^2 \mathbf{M}\hat{\mathbf{\Phi}} + \omega \mathbf{C}\hat{\mathbf{\Phi}} + \mathbf{K}\hat{\mathbf{\Phi}} = 0, \tag{13}$$

where $\hat{\mathbf{\Phi}} = [\hat{\Phi}_{-N}, \hat{\Phi}_{-N+1}, ..., \hat{\Phi}_N]^T$, $\mathbf{M}$ is the identity matrix, $\mathbf{C}$ depends on ω_m, and $\mathbf{K}$ depends on $\hat{a}$, ω_m, and k. For example, if $N = 1$ then the matrix elements in Eq. (13) are

$$\left(\omega^2 \begin{bmatrix} 1 & 0 & 0 \\ 0 & 1 & 0 \\ 0 & 0 & 1 \end{bmatrix} + \omega \begin{bmatrix} -2\omega_\mathrm{m} & 0 & 0 \\ 0 & 0 & 0 \\ 0 & 0 & 2\omega_\mathrm{m} \end{bmatrix} - \frac{k^2}{b} \begin{bmatrix} \hat{a}_0 - \omega_\mathrm{m}^2 & \hat{a}_{-1} & 0 \\ \hat{a}_1 & \hat{a}_0 & \hat{a}_{-1} \\ 0 & \hat{a}_1 & \hat{a}_0 - \omega_\mathrm{m}^2 \end{bmatrix} \right) \begin{bmatrix} \hat{\Phi}_{-1} \\ \hat{\Phi}_0 \\ \hat{\Phi}_1 \end{bmatrix} = 0. \tag{14}$$

As an example, consider the propagation of longitudinal waves in a bar with constant density $b = \rho_0$ and a time-varying Young's modulus $a(t) \to E(t)$, where $E(t)$ varies as a square wave with minimum value E_1 and maximum value E_2, which is written as

$$E(t) = E_1 + \Delta E H[\cos(\omega_m t)], \tag{15}$$

where $H(\cdot)$ is the Heaviside function, and $\Delta E = E_2 - E_1$. The Fourier coefficients in Eq. (10) are then

$$\hat{E}_n = E_2\delta_{n0} - \frac{\Delta E}{2}\text{sinc}(\frac{n\pi}{2}), \tag{16}$$

where $\text{sinc}(x) = \sin(x)/x$ and δ_{n0} is the Kronecker delta. The exact dispersion relation in this case is the equation [11]

$$\cos(\omega T) = \cos(kc_1T_1)\cos(kc_2T_2) - \frac{1}{2}\left(\frac{c_1T_1}{c_2T_2} + \frac{c_2T_2}{c_1T_1}\right)\sin(kc_1T_1)\sin(kc_2T_2), \tag{17}$$

where $T_1 = T_2 = \pi/\omega_\text{m}$, $T = T_1 + T_2$, and $c_{1,2} = \sqrt{E_{1,2}/\rho_0}$ [4]. This particular case has a similar dispersion form to the space-only dispersion relation, Eq. (7), except it is a function of time. Figure 2(a) compares the dispersion relation computed using Eq. (13) with parameters $N = 5$, $\omega_\text{m} = 1$, $E_1 = 1$, $E_2 = 3$, $\rho_0 = 1$ and two branches of the exact dispersion relation, Eq. (17). Note that the dispersion curves in Fig. 2(a) are periodic in frequency with respect to the modulation frequency ω_m, which is the analogue to wavenumber periodicity in the case of a spatially-varying modulus. The computed dispersion relation using Eq. (13) agrees well with the exact dispersion curves, and better agreement is obtained, particularly in the higher frequencies, by increasing the number of Fourier terms N. It is observed from Fig. 2(a) that this system exhibits wavenumber gaps, which are the analog of bandgaps in frequency for the the case of a spatially-varying modulus. However, propagating waves within the wavenumber bandgaps are unstable and exhibit infinite growth in amplitude in the lossless case [10].

The elements from the computed eigenvector $\hat{\Phi}$ are the amplitudes of the plane waves in Eq. (9). One also notes that the total energy of the propagating waves, which is related to the squared magnitude of the plane wave amplitudes, are not evenly distributed across each frequency. This can be represented on a frequency-wavenumber spectrum by weighting each curve by the magnitude of the fundamental plane wave amplitude $||\hat{\Phi}_0||^2$. Figure 2(b) depicts the same results as Fig. 2(a), but each curve is now assigned a color that represents the normalized magnitude of the fundamental $(m = 0)$ plane wave component in decibels, specifically $20\log_{10}(||\hat{\Phi}_0||/||\hat{\Phi}||)$. The main dispersion branch is now easily identifiable, as well as the branches that interact with the main branch near the wavenumber gaps.

2.3 Space- and time-dependent modulus

Finally, consider the case where now $a(x,t)$ is a periodic function of time and space. The solution techniques discussed for the time-only and space-only modulus cases can be leveraged to solve this general case. First, $a(x,t)$ is expanded as a Fourier series in time,

$$a(x,t) = \sum_{n=-N}^{N} \hat{a}_n(x)e^{-\text{i}n\omega_m t}, \tag{18}$$

where $\hat{a}_n(x)$ are the harmonic amplitudes and are periodic functions of space. As in the previous sections, a Bloch wave solution is assumed, where the Bloch mode $U(x,t)$ is now a periodic function of time and space,

$$u(x,t) = e^{\text{i}(kx-\omega t)}U(x,t). \tag{19}$$

Therefore, $U(x,t)$ can also be expanded as a Fourier series in time with harmonic amplitudes that are a periodic function of space

$$U(x,t) = \sum_{m=-N}^{N} \hat{u}_m(x)e^{-\text{i}m\omega_m t}. \tag{20}$$

Equation (1) is solved by substituting Eqns. (18)-(20) into Eq. (1), utilizing orthogonality of the Fourier series, and using the finite element method to discretize the resulting coupled ordinary differential equations that are a function of space into a quadratic eigenvalue problem

$$\omega^2\bar{\mathbf{M}}\boldsymbol{u} + \omega\bar{\mathbf{C}}\boldsymbol{u} + \bar{\mathbf{K}}\boldsymbol{u} = 0, \tag{21}$$

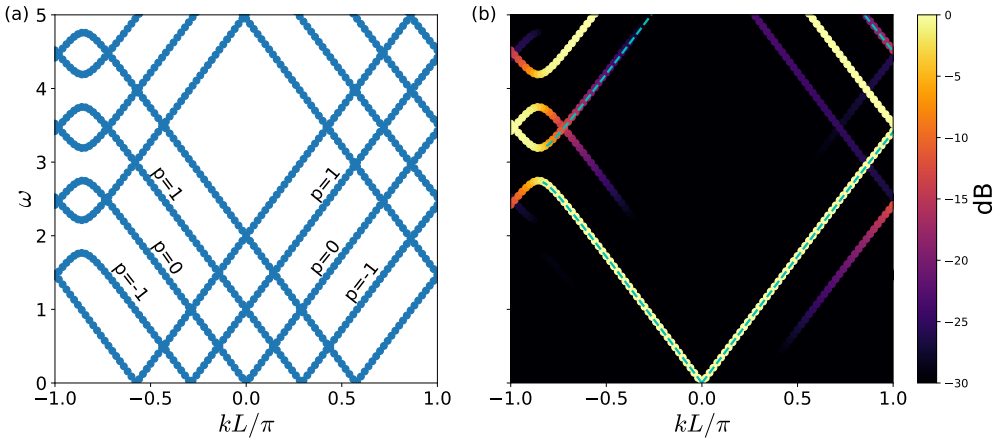

Figure 3. (a) Finite element computation of the dispersion relation for the case of translating material layers with modulation speed $c_m = 0.159$ ($\omega_m = 1$). Due to the bias in the $+x$ direction, the dispersion curves are not symmetric about $k = 0$, i.e. reciprocity is broken. (b) The dispersion curves shown in (a) but with each point colored by the magnitude of the fundamental component in decibels, $20\log_{10}(||\boldsymbol{u}_0||/||\boldsymbol{u}||)$. The dashed line is the first branch of the exact dispersion relation for this case, which is obtained using Eq. (26) and Eq. (7).

where $\boldsymbol{u} = [\hat{u}_{-N}, ..., \hat{u}_N]$ and $\hat{u}$ is discretized in space on a computational mesh, $\bar{\mathbf{M}}$ is the global assembly of the finite element mass matrices, $\bar{\mathbf{C}}$ is the global assembly of the finite element matrices proportional to ω, and $\bar{\mathbf{K}}$ is the global assembly of the finite element stiffness matrices.

As an example, consider the case of longitudinal wave propagation in a bar with constant density $b = \rho_0$ composed of periodic alternating layers from Sec. 2.1, now translating in the $+x$ direction at speed $c_m = \omega_m/k_m$, where $k_m = 2\pi/\lambda_m$ is the modulation wavenumber. Therefore, the Young's modulus $a(x,t) \to E(x,t)$ has the following functional form, which was recently studied using a different approach by Trainiti and Ruzzene [1]

$$E(x,t) = E_1 + \Delta E H\left[\cos\left(k_m x - \omega_m t\right)\right], \tag{22}$$

which is a generalization of the time-varying Young's modulus, Eq. (15). The Fourier coefficients in Eq. (18) are thus given by [1]

$$\hat{E}_n = \left(E_2\delta_{n0} - \frac{\Delta E}{2}\operatorname{sinc}\left[\frac{\pi n}{2}\right]\right)e^{ink_m x}. \tag{23}$$

The exact dispersion relation in this case can be obtained by shearing the dispersion relation for the case of spatial variation of the Young's modulus, Eq. (7). This is accomplished by replacing k with $\hat{k}$, ω with $\hat{\omega}$, and c_1, c_2 with $\hat{c}_1, \hat{c}_2$, where

$$\hat{c}_1 = c_1 - \frac{c_m^2}{c_1}, \tag{24}$$

$$\hat{c}_2 = c_2 - \frac{c_m^2}{c_2}, \tag{25}$$

and solving Eq. (7) with these transformed variables [11]. The variables $(\hat{k}, \hat{\omega})$ can be transformed back to (k, ω) with the following transformation,

$$k = \hat{k} + \frac{\hat{\omega}c_m L_1}{L(c_1^2 - c_m^2)} + \frac{\hat{\omega}c_m L_2}{L(c_2^2 - c_m^2)}, \tag{26}$$

$$\omega = \hat{\omega} + c_m\hat{k} + \frac{\hat{\omega}c_m^2 L_1}{L(c_1^2 - c_m^2)} + \frac{\hat{\omega}c_m^2 L_2}{L(c_2^2 - c_m^2)}. \tag{27}$$

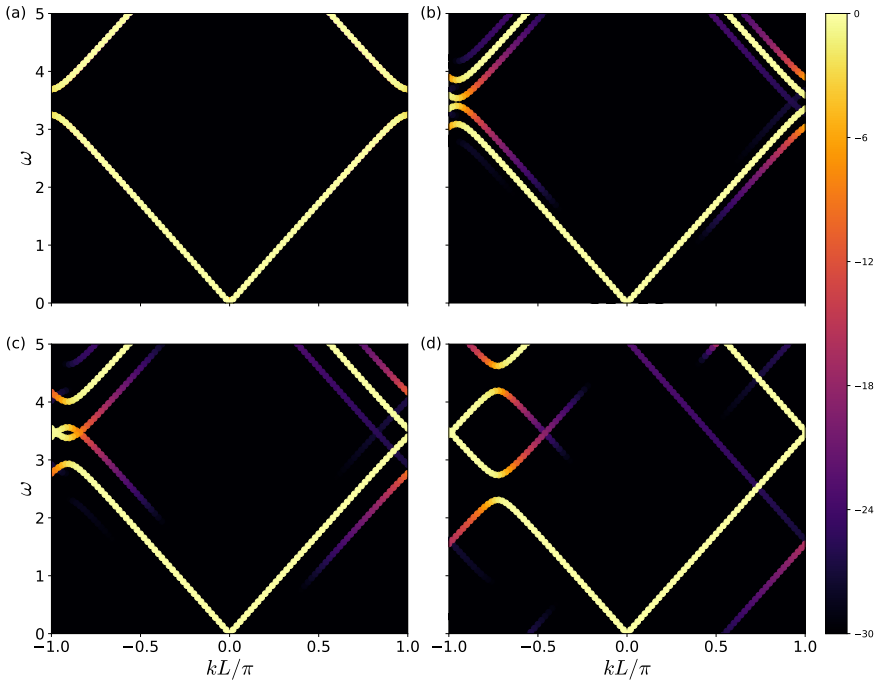

Figure 4. Dispersion relations for the translating layers case as a function of the modulation speed c_m. (a) No translation, $c_\mathrm{m} = 0$, (b) $c_\mathrm{m} = 0.05$, (c) $c_\mathrm{m} = 0.1$, (d) $c_\mathrm{m} = 0.3$.

Figure 3(a) shows the dispersion calculation from the finite element model using the parameters $E_1 = 1$, $E_2 = 1.5$, $\rho_0 = 1$, $L = 1$, $P = 2$, and $\omega_\mathrm{m} = 1$. As in the time-only modulation case, the entire frequency spectrum can be generated by translating the fundamental ($p = 0$) branch by $\pm p\omega_\mathrm{m}$. A bias in space-time has now been introduced in the $+x$ direction, which breaks time-reversal symmetry, and the dispersion relation is no longer symmetric about the $k = 0$ axis. Therefore, reciprocity is broken. Figure 3(b) shows the same dispersion curves as in Fig. 3(a), but with each point assigned a color determined by the magnitude of the fundamental component in decibels, specifically $20\log_{10}(||\hat{\boldsymbol{u}}_0||/||\boldsymbol{u}||)$. As in the time-only modulation case, it is evident from this plot that the harmonic amplitudes for each plane wave in Eq. (20) are not equal. This representation now shows what appears to be directional bandgaps in the $-x$ direction that do not exist in the $+x$ direction. These bandgaps are not identical to bandgaps in a system with only a spatially-varying modulus, since stable modes do exist within the bandgap. It can be seen from Fig. 3(b) that the branch with the largest magnitude agrees with the exact dispersion relation computed using the transformed variables, Eq. (26) and Eq. (7).

The frequency ranges of the directional bandgaps can be tuned with the speed of the modulation, c_m. Figure 4 depicts the changes in the dispersion relation as c_m is increased. For low modulation speed, mode splitting occurs and the spatial-only dispersion solution splits into the $\pm\omega_\mathrm{m}$ curves [12]. For a modulation speed of $c_\mathrm{m} = 0.1$, the band gap in the $+x$ direction closes, and the band gap in the $-x$ direction splits into two directional band gaps, where the lowest directional band gap translates down as the modulation speed is increased, and the higher directional band gap translates up in frequency as the modulation speed is increased. The width of the band gap can be tuned in the same way as the spatial-only modulation case, by increasing the contrast (ΔE) between layers.

3 SUMMARY

In this work, we have derived a computational approach based on the finite element method to study wave propagation in modulated media. The effects of space-only and time-only modulation of the material modulus on the propagation of Bloch waves in an elastic bar were explored, and the computational techniques used for these cases were combined to study the case of a space- and time-varying material modulus. It is straightforward to generalize this approach to the general elastodynamic case to study non-reciprocal wave propagation in a mechanically-modulated medium [3].

ACKNOWLEDGEMENTS

This work supported by National Science Foundation EFRI award no. 1641078 and the postdoctoral fellowship program at Applied Research Laboratories at The University of Texas at Austin.

REFERENCES

[1] Trainiti, G.; Ruzzene, M. Non-reciprocal elastic wave propagation in spatiotemporal periodic structures. New Journal of Physics, Vol 18 (8), 2016, 083047.

[2] Wallen, S. P.; Haberman, M. R. Nonreciprocal wave propagation in spring-mass chains with effective stiffness modulation induced by geometric nonlinearity. Physical Review E, Vol 99, 2019, 013001.

[3] Goldsberry, B. M.; Wallen, S. P.; Haberman, M. R. Non-reciprocal wave propagation in mechanically-modulated continuous elastic metamaterials. Journal of the Acoustical Society of America, In press.

[4] Brillouin, L. Wave Propagation in Periodic Structures: Electric Filters and Crystal Lattices. Courier Corporation, 2003.

[5] Hussein, M. I.; Leamy, M. J.; Ruzzene, M. Dynamics of phononic materials and structures: Historical origins, recent progress, and future outlook. Applied Mechanics Reviews, Vol 66(4), 2014, 040802.

[6] Adams, S. D.; Craster, R. V.; Guenneau, S. Bloch waves in periodic multi-layered acoustic waveguides. Proceedings of the Royal Society A, Vol 464 (2098), 2008, 2669–2692.

[7] Langlet, P.; Hladky-Hennion, A.; Decarpigny, J. Analysis of the propagation of plane acoustic waves in passive periodic materials using the finite element method. Journal of the Acoustical Society of America, Vol 98 (5), 1995, 2792–2800.

[8] Degraeve, S.; Granger, C.; Dubus, B.; Vasseur, J. O.; Pham Thi, M.; Hladky-Hennion, A. C. Bragg band gaps tunability in an homogeneous piezoelectric rod with periodic electrical boundary conditions. Journal of Applied Physics, Vol 115 (19), 2014, 194508.

[9] Deymier, P. A. Acoustic Metamaterials and Phononic Crystals. Vol 173, Springer Science & Business Media, 2013.

[10] Torrent, D.; Parnell, W. J.; Norris, A. N. Loss compensation in time-dependent elastic metamaterials. Physial Review B, Vol 97 (1), 2018, 014105.

[11] Nassar, H.; Xu, X.; Norris, A. N.; Huang, G. Modulated phononic crystals: Non-reciprocal wave propagation and Willis materials. Journal of the Mechanics and Physics of Solids, Vol 101, 2017, 10–29.

[12] Fleury, R.; Sounas, D. L.; Sieck, C. F.; Haberman, M. R.; Alù, A. Sound Isolation and Giant Linear Nonreciprocity in a Compact Acoustic Circulator. Science. Vol 343 (6170), 2014, 516–519.